Characterization of vascular permeability using a biomimetic microfluidic blood vessel model

Antony Thomas,[1,a)] Shunqiang Wang,[2,a)] Salman Sohrabi,[2,a)] Colin Orr,[1] Ran He,[2] Wentao Shi,[1] and Yaling Liu[1,2,b)]
[1]*Bioengineering Program, Lehigh University, Bethlehem, Pennsylvania 18015, USA*
[2]*Department of Mechanical Engineering and Mechanics, Lehigh University, Bethlehem, Pennsylvania 18015, USA*

(Received 30 October 2016; accepted 8 February 2017; published online 3 March 2017)

The inflammatory response in endothelial cells (ECs) leads to an increase in vascular permeability through the formation of gaps. However, the dynamic nature of vascular permeability and external factors involved is still elusive. In this work, we use a biomimetic blood vessel (BBV) microfluidic model to measure in real-time the change in permeability of the EC layer under culture in physiologically relevant flow conditions. This platform studies the dynamics and characterizes vascular permeability when the EC layer is triggered with an inflammatory agent using tracer molecules of three different sizes, and the results are compared to a transwell insert study. We also apply an analytical model to compare the permeability data from the different tracer molecules to understand the physiological and bio-transport significance of endothelial permeability based on the molecule of interest. A computational model of the BBV model is also built to understand the factors influencing transport of molecules of different sizes under flow. The endothelial monolayer cultured under flow in the BBV model was treated with thrombin, a serine protease that induces a rapid and reversible increase in endothelium permeability. On analysis of permeability data, it is found that the transport characteristics for fluorescein isothiocyanate (FITC) dye and FITC Dextran 4k Da molecules are similar in both BBV and transwell models, but FITC Dextran 70k Da molecules show increased permeability in the BBV model as convection flow (Peclet number > 1) influences the molecule transport in the BBV model. We also calculated from permeability data the relative increase in intercellular gap area during thrombin treatment for ECs in the BBV and transwell insert models to be between 12% and 15%. This relative increase was found to be within range of what we quantified from F-actin stained EC layer images. The work highlights the importance of incorporating flow in *in vitro* vascular models, especially in studies involving transport of large size objects such as antibodies, proteins, nano/micro particles, and cells. *Published by AIP Publishing.* [http://dx.doi.org/10.1063/1.4977584]

INTRODUCTION

Blood vessels are permeable, which allows for transportation of small molecules such as water, ions, nutrients, and even whole cells across the vessel. This capability is called vessel permeability.[1] Endothelial cells (ECs) line the blood vessel lumen and form a semi-permeable barrier through cell-cell junctions. Basal level vascular permeability is essential in the selective transport between blood and the interstitial space of organs. Such a permeability barrier is maintained through tight cell-cell junctions and is controlled by growth factors, cytokines, and

[a)]Electronic addresses: antonyt210@gmail.com; sqwang1990@gmail.com; and sas713@lehigh.edu
[b)]Author to whom correspondence should be addressed. Electronic mail: yal310@lehigh.edu, Tel.: +1-610-758-5839, Fax: +1-610-758-6224.

other stress related molecules.[2] Disruptions in the EC layer barrier can result in increased permeability. On detection of a potentially harmful substance, foreign organisms, or injured tissue, the permeability of blood vessels increases, which supplies plasma protein to the extravascular compartment in need of repair. This increase is controlled by several inflammatory mediators (e.g., vascular endothelial growth factor-A, tumor necrosis factor-α (TNF-α), Interleukin-6, Interleukin-1β, and thrombin) and delivers immunoglobulins, anti-proteases, constituents of the complement and coagulation systems, and other acute phase proteins to the site in order to act in local host defense and initiate tissue repair.[3,4]

Vascular permeability is a dynamic process and is mediated by acute or chronic exposure to inflammatory agents.[5–7] Permeability has also been found to be influenced by numerous (at least 25) gene products.[8] However, the dynamic nature of vascular permeability and external factors involved is still elusive. In this work, we use thrombin to induce permeability on EC layer based *in vitro* blood vessel models. Thrombin is an acute vascular inflammatory agent that induces blood coagulation and triggers specific stimuli on the EC layer, leading to intercellular gap formation and release of inflammatory mediators, vaso-regulatory agents, and growth factors.[9]

Scientists have employed both *in vivo* and *in vitro* platforms to understand the underlying mechanisms behind the above mentioned phenomena. *In vivo* works often require complex mammalian models and time-consuming surgical protocols, making them an expensive and challenging platform. These studies also raise ethical issues, and their resulting models respond differently to humans since interspecies predictability is low in response to drugs and diseases.[10] *In vivo* studies also only allow for a limited control of the heterogeneous parameters influencing the blood vessel and present challenges to real time imaging.[11] Relatively simpler and traditional *in vitro* platforms measure the flux of molecules of various sizes using transwell insert based permeability assays.[12–16] Such works are mostly performed under static conditions without consideration to the fluid shear stress (FSS) conditions that the endothelium is exposed to *in vivo*. Microfluidic technologies bring in a suite of new possibilities for blood vessel platforms. A couple of recent works used an endothelial cell layered microfluidic device to study permeability, but these works were performed on a cell layer not exposed to physiologically relevant flow.[17,18] Another work uses an endothelial cell layer to study monocyte adhesion and transmigration.[19]

Blood vessel endothelium is constantly exposed to FSS at its apical side due to blood flow. The mechanical stress generated on the EC layer due to this flow is an important extrinsic factor capable of modifying vessel barrier properties through alteration of the inter-endothelial junctions and the EC-extracellular matrix interactions.[20–23] It can also activate intracellular signaling events, altering barrier properties like increased intracellular Ca^{2+} levels and the generation of inositol trisphosphate,[24–26] activation of Rac,[27,28] RhoA-dependent reorganization of the actin cytoskeleton,[21,22,29] and β_1-integrin-dependent increases in caveolin-1 phosphorylation.[21] Therefore, integration of *in vivo* levels of flow with the EC culture is important in limiting the chances of the cell monolayer undergoing phenotypic drifts and no longer reflecting *in situ* characteristics. An *in vitro* blood vessel model that can sustain EC culture under native conditions and can evaluate the dynamics and heterogeneous nature of vascular permeability in real time when triggered by an inflammatory agent holds huge potential.

This work studies the dynamics of increases in EC layer permeability during thrombin treatment in a biomimetic blood vessel (BBV) microfluidic model and a transwell insert model. The *in vitro* BBV platform consists of an upper and lower microfluidic channel separated by a semi-permeable membrane. Bovine aortic endothelial cells (BAOECs) were cultured on the semi-permeable membrane under *in vivo* levels of flow. In order to study the increase in vascular permeability during inflammation in the BBV and transwell insert model, the monolayer of BAOECs was exposed to media spiked with thrombin and a tracer molecule. Thrombin treatment leads to EC layer F-actin cytoskeletal filament rearrangement, which in turn increases permeability. The change in vascular permeability was quantified using a tracer molecule based assay. This system is based on determining the amount of fluorescein isothiocyanate (FITC)-dye and FITC-Dextran (4k Da and 70k Da) molecules that permeates from the upper to the

lower channel through the EC intercellular gaps and membrane. The amount of dye molecules that permeated were collected in real time and measured spectrophotometrically to quantify the process. An analytical permeability model was used in this work that distinctly identifies and compares the permeability characteristics of the tracer molecules based on their transportation nature (diffusion or convection depended) for the two platforms. This helped us in identifying the similarities in permeability characteristics of ECs cultured in both platforms and also in understanding the scenario where using a flow integrated vascular model would be important. In this work, we also calculated the relative increase in endothelial intercellular gap area during thrombin treatment from the permeability data. This relative increase was compared to the increase in intercellular gap area calculated from EC F-actin immunofluorescence images. A computational model of the BBV model was also developed to understand how dye molecules with different sizes transport through the porous membrane under flow. This work analyzes the permeability of tracer molecules of different sizes in two different models and highlights the similarities and differences in the permeability characteristics of the EC layer between the two models. It also highlights the need for flow integrated vascular models, especially in studies where larger sized molecules are involved, whose flow transport is convection dominated.

MATERIALS AND METHODS

Fabrication and EC culture on BBV model

Channels were made of polydimethylsiloxane (PDMS) from a photolithographically patterned silicon wafer, and a monolayer culture of BAOECs was attained as explained in our prior work.[30] The upper and lower channels were cast out of Sylgard 184 PDMS (Dow Corning Corp.). The upper channel was 20 mm long, 350 μm wide, and 100 μm tall, and the lower channel was 5 mm long, 1000 μm wide, and 100 μm tall. A polycarbonate (PC) track-etched, thin, and clear membrane (Whatman, GE Healthcare) with 1 μm diameter pores and an average calculated pore density of 1.5×10^7 pores/cm^2 was embedded between the two PDMS channels. The bottom PDMS channel was bonded onto a glass slide by exposing the sides in contact to oxygen plasma. The upper PDMS channel was bonded to the membrane by using a thin PDMS mortar film (10:1 ratio of base and curing agent with toluene in equal proportion). The upper channel bonded to the membrane was then bonded to the lower channel after making sure the channels are aligned well. After each step, the components were placed in an oven at 60 °C for 10 min to enhance bonding. Inlet and outlet ports were punched to provide access to upper and lower channels.

Once fabricated, the devices were sterilized overnight under UV light to prepare for cell culture. Prior to cell seeding, the upper channel and membrane of the device were coated with 50 μg/ml fibronectin (Sigma-Aldrich) overnight at 37 °C. BAOECs were seeded by placing a 20 μl drop of media containing cells at a density of 2×10^7 cells/ml in the channel inlet. Cells flow from the inlet to the outlet and, upon reaching equilibrium, settle down and attach on the semi-permeable membrane. Cell seeded devices were placed in an incubator under standard culture conditions (37 °C and 5% CO^2) overnight to allow cell attachment and spreading on the membrane. Upon reaching confluence, the BAOECs were subjected to a physiologically relevant FSS of 12 dyne/cm^2.[31,32] The flow was enabled using a high precision and extremely low pulsation peristaltic pump (ISMATIPC-N series), and the entire setup was placed in standard culture conditions. Recirculation of media was not permitted while thrombin and tracer molecules were passed through the channels. To calculate the volumetric flow rate that corresponds to the required maximum FSS experienced by the ECs, the following equation was used:[33]

$$\tau_{cell} = \frac{6\mu Q}{wh^2}\left(1 + \frac{h}{w}\right) f\left(\frac{h}{w}\right). \quad (1)$$

Here, "h" and "w" are the height and width of the microfluidic channels, respectively."τ_{cell}" is the FSS experienced on the cell surface in the channel. "μ" = 0.007 dyne s/cm^2 is the fluid viscosity for the medium at 37 °C, and Q is the volumetric flow rate. "f" is a geometry factor

derived from the ratio of width and height. "*f*" has been calculated to be 0.74 for the current channel geometry.

Permeability assay in BBV model

BAOECs were treated with thrombin at a concentration of 1 Unit (U)/ml after being subjected to 6 h or more of flow in the BBV model. Thrombin induces an acute inflammatory response on ECs and leads to profound increases in cell monolayer permeability. Thrombin was mixed with flow media, along with the tracer molecule, and the treatment was performed under flow on the apical side of the cells. Fluorescent FITC sodium salt (376 Da), FITC-Dextran 4k Da, and FITC-Dextran 70k Da molecular weights were used as tracer molecules. FITC sodium salt was flown at 0.625 mg/ml and the FITC-Dextran molecules at 5 mg/ml. We chose different working concentrations as the lower molecular weight FITC dye at 0.625 mg/ml had comparable fluorescent intensity to FITC-Dextran 4k Da and 70k Da at 5 mg/ml. This permitted ease in spectrophotometric detection and analysis. The extent of tracer molecule permeation to the abluminal lower channel is a direct indication of the level of vessel permeability, which was monitored in real time by withdrawing 6 μl samples from the outlet of the lower channel every 10 min. These samples were analyzed spectrophotometrically using an Infinite 200 PRO NanoQuant microplate reader at 490 nm excitation and 521 nm emission. The volume of buffer solution in the lower channel was maintained by adding 6 μl of phosphate buffered saline (PBS) to the inlet before withdrawing the sample. It was important to make sure that sample mixing between time points was minimal and this was ensured by measuring the amount of tracer molecule remaining after data sample withdrawal for a few cases using confocal microscopy and spectroscopy. Supplementary material Figure S4 shows confocal images of leftover FITC dye in the lower channel before and after 6 μl data sample elution, showing the amount of tracer dye leftover to be minimal between each time points. The dosage and treatment time for thrombin to induce an increase in permeability on BAOECs was determined from other studies[34–37] and by performing cell permeability assays on transwell inserts.

Permeability assay in transwell insert model

For the transwell insert model, the BAOECs were seeded at a density of 2×10^4 cells in the luminal chamber of ThinCert transparent inserts for 12-well plates a membrane with 1 μm diameter pores. Cells were cultured in Dulbecco's modified eagle medium (DMEM) with 10% heat inactivated fetal bovine serum. On reaching confluence, the cells were treated with thrombin by replacing the medium in the luminal side with fresh DMEM (1% heat inactivated serum) supplemented with thrombin and tracer molecule. Media volumes of 1500 μl and 500 μl were maintained in the abluminal and luminal sides, respectively, to make sure the hydrostatic pressure between the chambers remained constant. 750 μl of media from the abluminal chamber was replaced every 10 min, and the presence of tracer molecules was monitored spectrophotometrically. To keep the permeability assay protocol in the BBV platform and the transwell insert study similar, the supplemented media in the luminal chamber was also replaced every 10 min to ensure a fresh and constant supply of thrombin and tracer molecules.

Rearrangement of actin filaments

The rearrangement of F-actin stress fibers was studied to understand the correlation between the increase in vessel permeability and F-actin cytoskeletal arrangement patterns on thrombin treatment. Confluent cell monolayers were treated with 1 U/ml thrombin in DMEM medium (1% heat inactivated serum) for various lengths of time. The static case was performed on ECs cultured on fibronectin coated cover slips. For the flow case, thrombin was spiked along with flow media in the BBV model. After thrombin treatment, the cells were fixed with 3.7% paraformaldehyde (Sigma) for 20 min and permeabilized with 0.5% Triton X-100 (Sigma) for 3 min. Cells were washed with PBS between each step and were finally stained with 50 μg/ml FITC-phalloidin (Thermo Fisher Scientific Inc.) solution in PBS for processing by immunofluorescence

microscopy. Observations were made with a fluorescent confocal microscope (FV1000-IX81, Olympus), and image analysis was performed using ImageJ software.

Statistical analysis

The results are an average from three independent experiments with a p-value <0.05. The results are presented as the mean $\pm$ the standard deviation. An unpaired Student t test was used to analyze statistical differences between control and treated groups. Differences were considered statistically significant at $p < 0.05$.

Analytical model

Dye transport across the EC layer is a combination of both diffusive and convective flux within intercellular gaps and membrane pores. By looking into the Peclet number, we can better understand the underlying mechanism in the transport process of tracer molecules through the intercellular gap. The Peclet number can be expressed as

$$\mathrm{Pe} = \frac{\mathrm{L_{EC}}\,\bar{\mathrm{u}}}{\mathrm{D_{eff}}}, \tag{2}$$

where "$\mathrm{L_{EC}}$" is the EC layer thickness, "$\bar{\mathrm{u}}$" is the average velocity within the membrane pore, and "$\mathrm{D_{eff}}$" is the effective diffusion of dye molecules. Convective flux can be created by hydrostatic or osmotic pressure difference according to the Starling and Kedem-Katchalsky equations[38]

$$\mathrm{J_v} = \mathrm{Lp}(\Delta \mathrm{P_T} - \sigma_\mathrm{s}\Delta\pi), \tag{3}$$

where "Lp" is the hydraulic conductivity, "σ_s" is the osmotic reflection coefficient, and "$\Delta \mathrm{P_T}$" and "$\Delta\pi$" are the hydrostatic and osmotic pressure differences across the EC layer, respectively.

Furthermore, to compare BBV and transwell insert models, all the test parameters should be the same or properly normalized. Here, we used an analytical model that considers the major differences between the two platforms during tracer molecule collection in the lower channel; i.e., the surface area permitting tracer molecule permeation and assay volumes. Based on this, the permeability can be expressed as:

$$P = (\Delta C_L V_L)/(C_U A \Delta t), \tag{4}$$

where "ΔC_L" is the concentration change in the lower channel, "V_L" is the volume of sample media, "C_U" is the concentration in the upper channel, "A" is the area of the membrane that allows fluorescent tracers to permeate, and "Δt" is the assay time.

The real-time permeability data after thrombin treatment can also be used to calculate the relative intracellular gap area. Assuming diffusion dominant dye transport through the EC layer, the tracer flux to the abluminal chamber can be expressed as

$$\frac{C_L}{\Delta \mathrm{t}} V_L = D\frac{(C_U - C_L)}{L_{EC}} A_{gap}, \tag{5}$$

where "L_{EC}" is the cell layer thickness and "A_{gap}" is the intracellular gap area overlapping the pores of the membrane. Therefore, the relative intracellular gap area can be estimated as

$$A_{rel-gap} = \frac{A_{gap}}{\phi \times A_{mem} \times \pi \times {r_{pore}}^2} \times 100, \tag{6}$$

where "A_{mem}" is the membrane surface area and "ϕ" and "r_{pore}" are the porosity and pore radius of the membrane, respectively. In the following Results and Discussion Section, these analytical formulations are used to post-process and help analyze real-time permeability data.

Finite element simulation

A computational model was used to examine the molecule transport across the endothelial monolayer in the microfluidic chip.[39] Transient analysis of the molecule concentration was performed in a model with prescribed actual dimensions. Tetrahedral mesh elements were used in this work with minimum element quality smaller than 0.25. The mesh quality was also confirmed by using finer mesh elements, which yielded a concentration difference smaller than 1.5%.

To mimic the inflammatory effect in ECs, various effective pore diameters, i.e., 200 nm, 400 nm, 800 nm, and 1 μm (actual membrane pore diameter), with a porosity of 5% were used to understand how dye molecules with different sizes transport through the porous membrane.

The convection-diffusion equation was used to predict the molecule transport as follows:

$$\frac{\partial \mathrm{c}}{\partial \mathrm{t}} + \nabla \cdot (-\mathrm{D}\nabla \mathrm{c}) = -\mathrm{u} \cdot \nabla \mathrm{c}, \tag{7}$$

where "c" is the molecule concentration, "u" is the flow velocity, and "D" is the diffusion coefficient. The diffusion coefficients are $2.7 \times 10^{-10}\,\mathrm{m^2/s}$, $1.35 \times 10^{-10}\,\mathrm{m^2/s}$, and $2.3 \times 10^{-11}\,\mathrm{m^2/s}$ for FITC dye, FITC Dextran 4k Da, and FITC Dextran 70k Da, respectively.[40,41] The total number of probe molecules collected can then be obtained by integrating the concentration over the bottom channel.

RESULTS AND DISCUSSION

On-chip cell culture

An intact blood vessel endothelium is constantly exposed to FSS at its apical side from blood flow. Therefore, integrating *in vivo* levels of flow to the EC culture is important in limiting the chances of the cell monolayer undergoing phenotypic drifts, and thus no longer reflecting *in situ* characteristics. After seeding the BAOECs in the upper channel of the BBV device and on reaching confluence after about 16 h (overnight incubation) of static culture, the ECs were subjected to a FSS of 12 dyne/cm^2 by flowing media at a flow rate of 3.7 μl/s. The confluence of the cell layer was ensured to be optimal (at least 90%) through phase contrast microscopy before tests were performed. Figure 1 has a photograph of the bi-layer device showing the upper and lower channel separated by the semi-permeable membrane with their inlets and outlets marked. Details on cell shape, F-actin filament alignment, and reorganization on exposure to FSS in this device have been reported in our previous work.[30] F-actin realignment to flow for BAOECs happens within 4 h in the BBV model (details in our previous work), and our permeability assay is performed 6 h after applying FSS in order to consider this.

In this work, we characterize changes in vascular permeability caused as part of an inflammatory response. The EC layer in the BBV model was treated with thrombin, an inflammatory agent. As explained in Figure 1(b), thrombin and tracer molecule were flowed along with media in the upper channel, thus inducing inflammatory response on the EC layer from its apical side. EC layer permeability increases during inflammation. This happens due to the increase of intercellular gap. The tracer molecule permeates through these gaps and the 1 μm diameter pores on the membrane toward the lower channel. The amount of the tracer molecule diffusing into the lower channel is a direct quantification of the extent of vessel permeability. In order to understand how introduction of flow influences permeability, we performed a time course study by flowing media mixed with FITC dye (0.625 mg/ml) at a FSS of 12 dyne/cm^2 on a confluent BAOEC layer for 6.5 h after 1 h of static culture (Figure 1(d)). Permeability of FITC dye remains constant during the first hour of static culture (comparable to the control case) but increases ~4 times with the onset of flow. After about 2.5 h of flow, the permeability reduces to a range comparable to initial static culture or control case and maintains the range for the rest of the time period. Similar permeability characteristics have

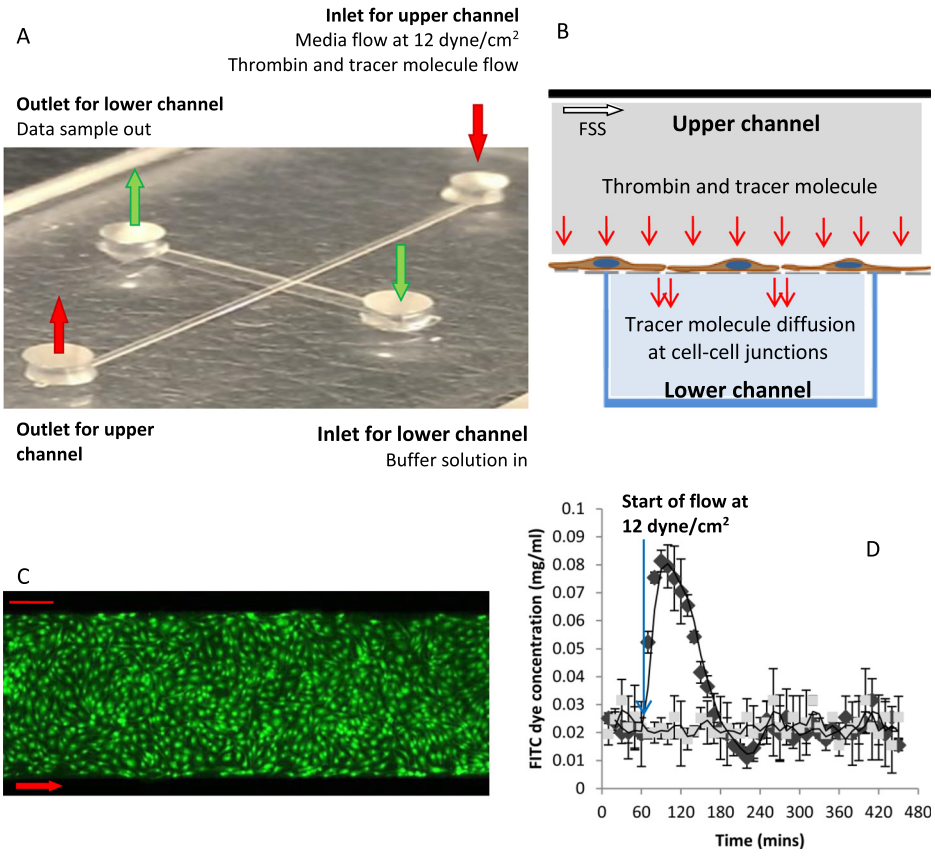

FIG. 1. (a) Photograph of the bi-layer device showing the upper and lower channel separated by the semi-permeable membrane along with their inlets and outlets. The apical side of the EC layer faces the upper channel and is exposed to media flow. Thrombin and tracer molecule are added to media to study blood vessel permeability under acute inflammation. Tracer molecule diffusion to the lower channel is controlled by the extend of EC permeability under inflammation. The diffused data sample is collected from the lower channel. (b) Schematic depicts EC growth on semi-permeable membrane, thrombin treatment from upper channel, and tracer molecule diffusion through intercellular gaps. (c) Fluorescence labeled actin cytoskeleton (FITC-phalloidin) image of confluent BAOEC layer aligned to flow (12 dyne/cm^2 FSS for 6 h) in the upper channel. Arrow shows the flow direction (Scale bar: 100 μm). (d) Time course for understanding permeability characteristics of a confluent BAOEC layer is performed by flowing media mixed with FITC dye (0.625 mg/ml) at a FSS of 12 dyne/cm^2 after 60 min of permeability check under static culture (dark grey marker). Permeability of FITC dye remains constant during the first 60 min of static culture but increases ~4 times with the onset of flow. After about 2.5 h of flow, the permeability reduces to a range comparable to initial static culture or control case (light grey marker) and stays within that range.

been reported previously for endothelial cells when they are exposed to FSS, where the permeability increases immediately at the onset of flow and slowly plateaus to a baseline value.[42,43]

The introduction of flow does bring about a transient increase in permeability for the BAOEC layer that stabilizes after about 2.5 h of flow. Thus, it is safe to assume that this study is performed on a BAOEC layer that has been primed to flow, and the study performed after 6 h of exposure to FSS will not be affected by any initial flow related changes in permeability.

Characterization of vascular permeability on BBV model

Figures 2(a), 2(b), and 2(c) show the permeability curve for FITC sodium salt, FITC-Dextran 4k Da, and FITC-Dextran 70k Da, respectively, along with the control case (no thrombin treatment). The tracer molecule concentration was quantified by comparing the fluorescence intensity of collected data samples to a concentration standard curve. For the three

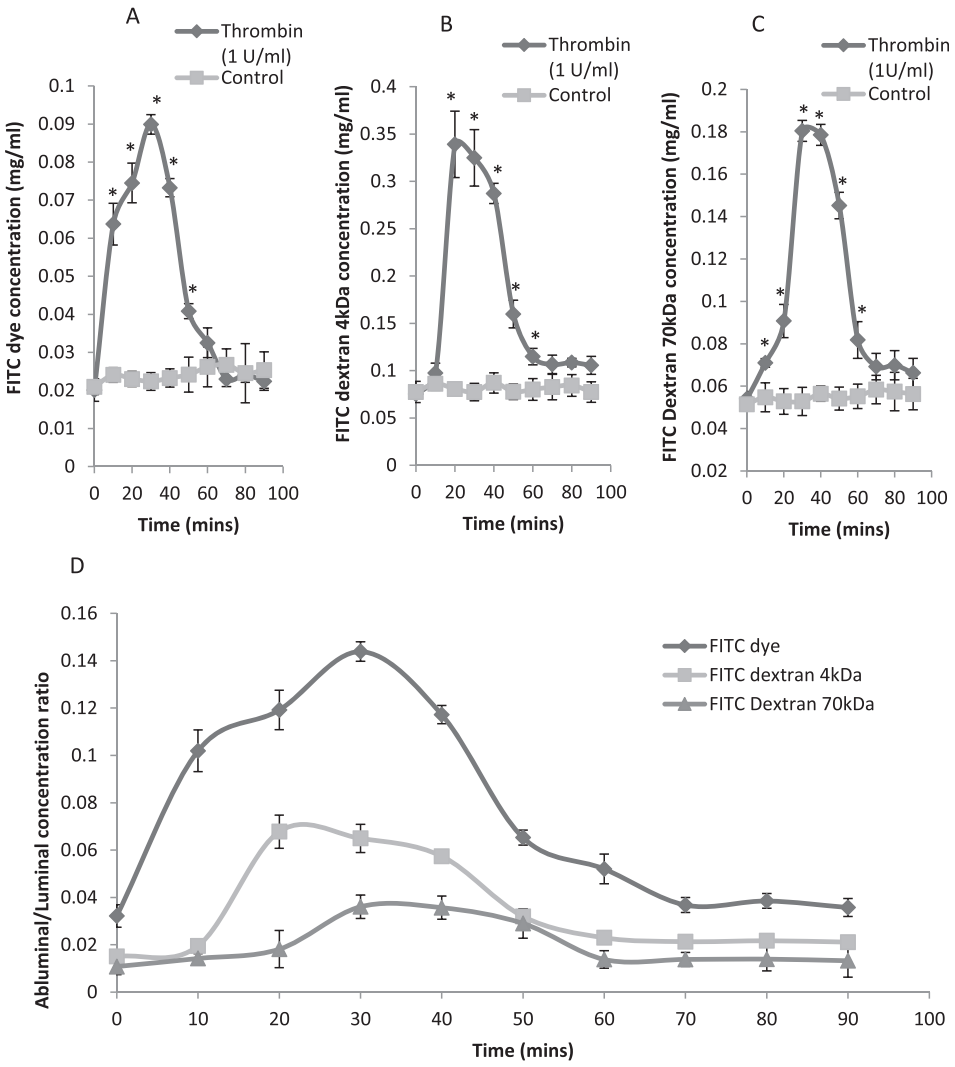

FIG. 2. Permeability of the tracer molecule through the EC layer in the biomimetic device. (a) Permeability of FITC dye through the EC layer when treated with thrombin at 1 U/ml compared to the control case. (b) Permeability of FITC dextran 4k Da through the EC layer when treated with thrombin at 1 U/ml compared to the control case. (c) Permeability of FITC dextran 70k Da through the EC layer when treated with thrombin at 1 U/ml compared to the control case. (d) Normalized comparison of FITC dye and FITC dextran 4k Da permeability on the EC monolayer when treated with thrombin at 1 U/ml. FITC dye with a lower molecular weight has higher permeability compared to FITC dextran 4k Da case. Asterisks indicate that the values are significantly different from control values ($p < 0.05$).

tracer molecules, it is observed that the concentration in the lower channel starts to increase acutely within 10 min of thrombin treatment and reaches the max value (0.09 mg/ml for FITC sodium salt, 0.34 mg/ml for FITC-Dextran 4k Da and 0.18 mg/ml for FITC-Dextran 70k Da) within 20–30 min. This means the permeability or gap formation of the EC monolayer initializes rapidly and reaches its maximum within 20–30 min. The tracer molecule concentration increases about 3.5 times, and this is a direct measurement of the change in vascular permeability. Then, a fall in concentration of tracer molecule in the lower channel is observed that plateaus to a minimum value by about 60–70 min. This signifies the decrease in EC layer permeability due to the reduction of intercellular gaps as a result of barrier recovery by the ECs after the acute increase in permeability. Thrombin induced vascular permeability dynamics of a similar nature in BAOECs have been elucidated in previous studies.[34–36,44,45]

Figure 2(d) compares the concentration ratio of the tracer molecules in the abluminal (lower) channel to their luminal (upper) channel concentration. For this, the concentration of

the tracer molecule in the abluminal channel is divided by the corresponding luminal concentration and compared along with thrombin treatment time. This normalizes the effect of doing the tests at different luminal concentrations to an extent and provides insight on how the size of the tracer molecule affects permeability. Also, the low concentrations used in this work lead to negligible interaction among molecule-tracers, which will make the permeability characteristics observed independent of molecule concentration. It is found that the permeability of tracer molecules across the ECs decreased with increasing molecular weight. The lower molecular weight FITC sodium salt diffused faster and in larger quantities through the intercellular gaps than the higher molecular weight FITC-Dextran 4k Da and 70k Da. Similar results have been previously observed in studies using tracer molecules of different sizes.[40,46–49] A reduction in diffusivity was observed with an increase in molecular weight of the tracer molecule.

Vascular permeability comparison on transwell inserts

We also analyzed the permeability of BAOEC layer when treated with thrombin on traditional transwell inserts and compared the permeability data to that generated on the BBV model. On transwell inserts, we maintained a static culture of ECs that were treated with thrombin upon reaching confluence. In the transwell study, only half of the total tracer molecules that permeated to the abluminal side were collected to prevent the cells from drying due to lack of media on the abluminal side and to remain consistent. As a result, each of the following readings would have leftover tracer molecules from the previous time point. We normalized this effect by mathematically subtracting the amount of tracer molecules leftover from the previous time point. Figures 3(a-i) and 3(a-ii) show that thrombin increased the permeability of the EC monolayer within 10 min for both FITC Dextran molecules, which reached a maximum after about 20–30 min. After this, we observed a fall in tracer molecule concentration, which signifies a decrease in endothelial permeability. The permeability is comparable to the control case within about 80 to 90 min of thrombin treatment for both tracer molecules.

The dynamics of vessel permeability observed in the BBV model and the traditional transwell system are similar. The recovery of endothelial barrier function was a steady and relatively slower process in the static transwell insert studies (about 80–90 min to plateau) compared to the flow integrated microfluidic platform (60–70 min). The time point for initial acute increase in permeability is similar for both these platforms, and the shorter recovery time for cell layer barrier integrity in the BBV model is likely due to the inclusion of flow. Later, we analytically compared the permeability data from these two models.

Peclet number based analysis of dye molecule transport

In the convection dominant conditions $(\mathrm{Pe} \gg 1)$, the transport is independent of tracer type with different diffusivity. Since our results for abluminal/luminal concentration ratios in Figure 2(d) change with dye type, it can be concluded that dye transport is not convection dominant. In the BBV case, a 3.7 μl/s flow rate induces 12 dyne/cm^2 of shear on ECs and a 500 Pa hydrodynamic pressure difference across membrane. This pressure difference creates a convective dye transport to the lower channel with an average velocity of 3×10^{-5} m/s. The Peclet number for FITC dye with a diffusion coefficient of 2.7×10^{-10} m^2/s is estimated as 0.2, which indicates that the transport process is mainly diffusion dominant. In other words, high hydraulic resistance due to small openings prevents convection of dye molecules to the lower channel. It should be mentioned that for FITC Dextran 70k Da, the Peclet number increases to $\sim$1 due to lower diffusivity. In this case, convection transport will be as important as diffusion.

Normalized analysis of permeability between BBV and transwell insert model

The transport of tracer molecules in the transwell case is mediated only by diffusion, but in the BBV model the transport is done by both diffusion and convective flux. A direct ratio based analysis (abluminal/luminal tracer molecule fluorescence intensity) in Figures 2 and 3 provides

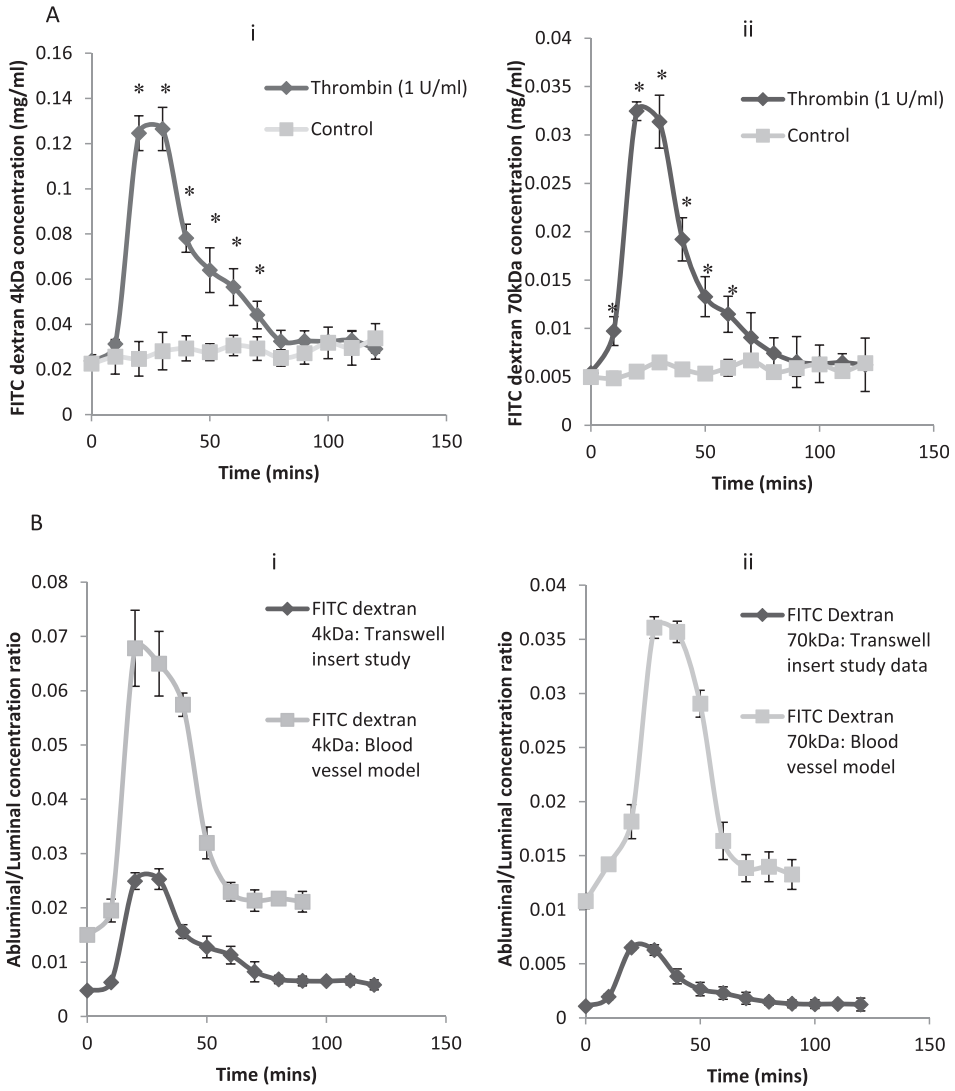

FIG. 3. (a) Permeability of tracer molecule through the EC layer in the transwell insert model study. Permeability of (i) FITC dextran 4k Da and (ii) FITC dextran 70k Da through the EC layer when treated with thrombin at 1 U/ml compared to the control case. (b) Normalized comparison of (i) FITC dextran 4k Da and (ii) FITC dextran 70k Da permeability on the EC monolayer in the BBV model and transwell insert case on thrombin treatment. EC monolayer in the biomimetic device recovers its barrier integrity within about 60 min compared to about 80 min in the transwell insert case. Asterisks indicate that the values are significantly different from control values ($p < 0.05$).

a platform specific understanding of the change in permeability based on the tracer molecule. On comparison of permeability between the BBV and transwell insert models (Figures 3(b-i) and 3(b-ii)) for FITC Dextran 4k Da and 70k Da cases, it is observed that the BBV model generates a higher proportion of permeability for both the tracer molecules. However, to compare two platforms, all the test parameters should be the same or properly normalized. As mentioned before, every 10 min, we took $V_L = 6\,\mu$l and $V_L = 750\,\mu$l samples from the BBV and transwell cases, respectively. Moreover, the surface area of membrane in the BBV and transwell cases was 0.35 mm^2 and 113 mm^2, respectively. Using Eq. (4), we are able to compare the permeability between two platforms as shown in Figure 4(a), and we understand that the smaller FITC-Dextran 4k Da tracer molecule has similar permeability in both the platforms. This aligns with the fact that FITC-Dextran 4k Da have a Peclet number <1 and thus follow diffusion dominated transport kinetics. This means that the particles are so small that convection of the tracer molecules is negligible and does not contribute towards its transport to the lower channel in the

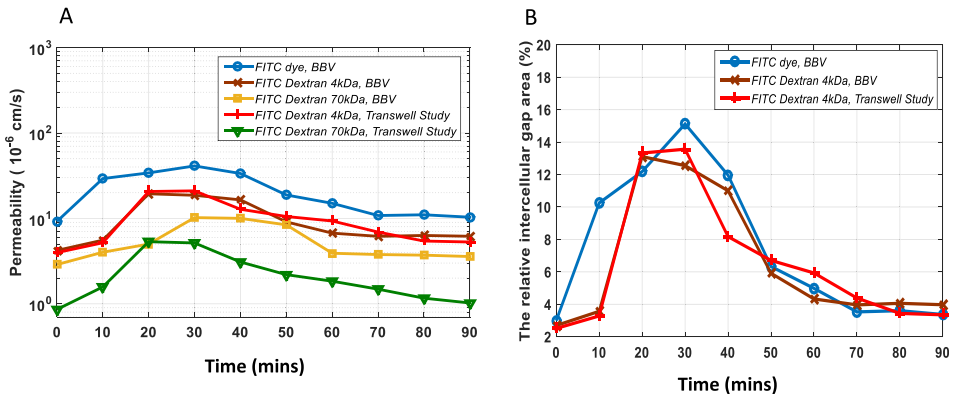

FIG. 4. (a) The permeability of the tracer molecule through the EC layer in the biomimetic device and the transwell insert study when treated with thrombin at 1 U/ml compared to the control case. (b) The relative intracellular gap area in EC layer in the biomimetic device and the transwell insert study when treated with thrombin at 1 U/ml compared to the control case.

BBV model. However, permeability of the larger FITC 70k Da Dextran tracer molecule is ∼2× greater in the BBV model compared to the transwell insert case (Figure 6). The reason for this observation is that the Peclet number is about "1" for this tracer molecule due to its larger size and thus has convection transport characteristics as well. Therefore, the convective flow in the BBV model enhances the 70k Da FITC-Dextran transport rate to the lower channel. So for analyzing the permeability/blood vessel transport of molecules larger than a certain size (having a Peclet number > 1, thus convection dominated transport characteristics), our BBV model provides a better fit due to the inclusion of flow effects.

Calculation of relative intracellular gap area

Using Eq. (6), the inflammatory response of the EC layer in terms of the relative intracellular gap area is calculated for BBV and transwell cases as shown in Figure 4(b). In all shown cases, the transport process is diffusion dominant, $Pe < 1$. The measured relative gap area using the FITC and FITC Dextran 4k Da tracer molecules was almost identical for both platforms. This means that the intercellular gap area induced by thrombin treatment does not change significantly with testing conditions (testing under FSS vs. static) and tracer molecule. Still, it should be noted that the overall transport rate and permeability strongly depend on these parameters as shown in Figures 2, 3, and 6. Therefore, the BBV study provides a more realistic understanding of transport phenomena *in vivo*. It should be noted that the relative intercellular gap area of the endothelial layer increases to be ∼12%–15% for dye transport after about 20–30 min of thrombin treatment as shown in Figure 4(b).

We further examined the F-actin remodeling under thrombin treatment of ECs in these two different platforms, to compare the transient nature of stress fiber alignment related to barrier integrity recovery.

F-actin cytoskeletal remodeling

Thrombin treatment of ECs leads to F-actin cytoskeletal filament formation and rearrangement. Thrombin induces myosin light chain phosphorylation and subsequent activation of acto-myosin based contractile systems. This leads to isometric tension development in the cell and thus EC retraction and an increase in vessel permeability.[50–53] After demonstrating the kinetics of EC monolayer permeability through tracer molecule transport in static (ECs cultured on transwell inserts) versus flow cases (ECs cultured in the BBV model), confocal microscopy and immunofluorescence staining were used to examine the changes in F-actin stress fiber arrangement after thrombin treatment (1 U/ml). Figures 5 and 6 show z-series composite micrographs of control and thrombin stimulated EC monolayers for both cases, respectively. The control case consists of a monolayer of ECs with tight intercellular contact and predominantly

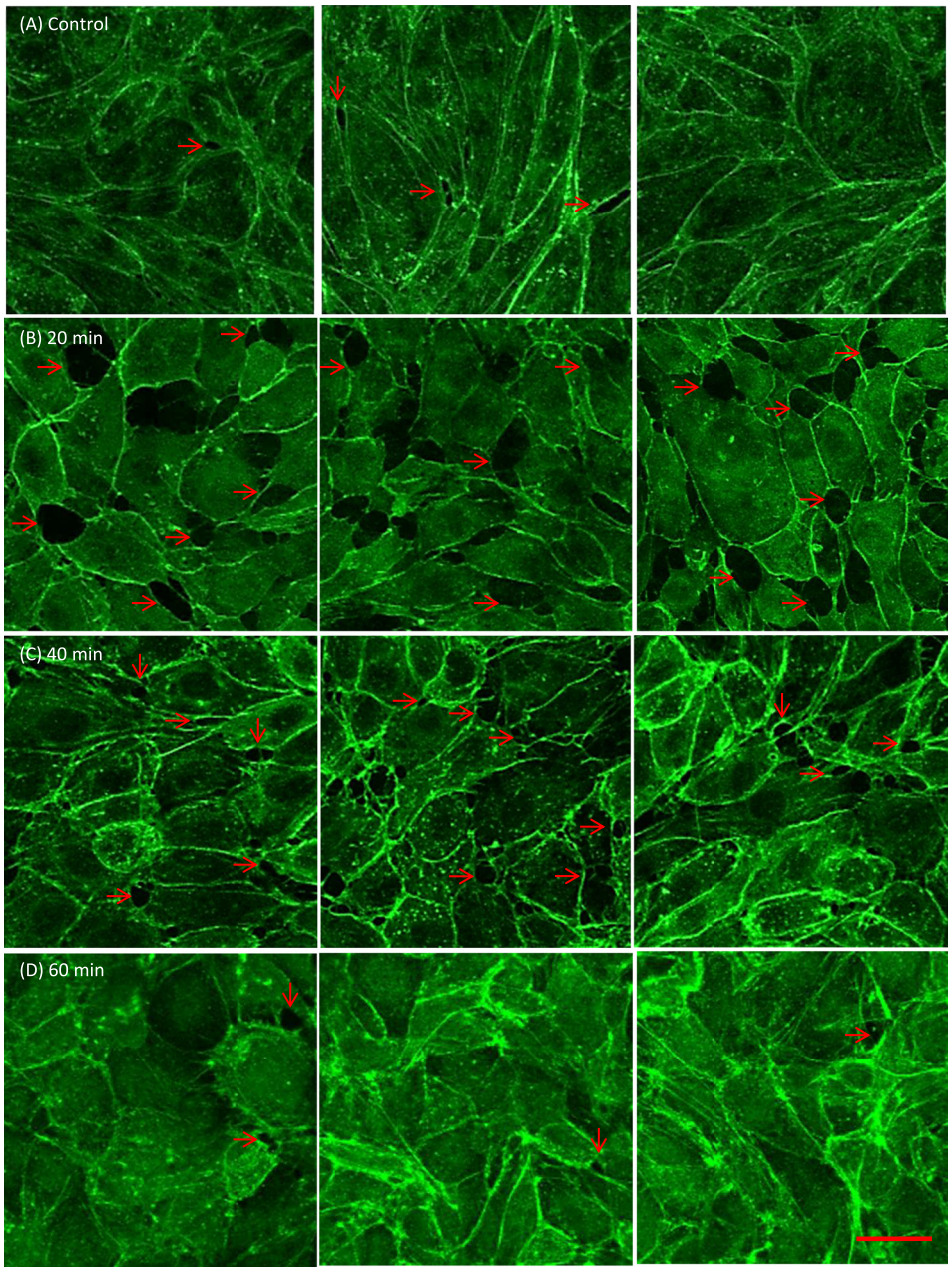

FIG. 5. Confocal Z-projections of thrombin induced F-actin remodeling on BAOECs cultured in the microfluidic biomimetic device under flow. (a) Control case only subjected to 6 h or more of flow at 12 dyne/cm^2. (b) 20 min of thrombin treatment at 1 U/ml produce regions without F-actin stress fibers between cells which signify inter-cellular gap formation. (c) These gaps tend to reduce and bridge by increased cortical actin presence towards cell periphery after 40 min of thrombin treatment. (d) There is steady presence of F-actin filaments on the cell monolayer after 60 min of thrombin treatment, signifying the decrease in inter-cellular gaps (Scale bar: 25 μm).

peripheral cortical actin. With thrombin stimulation, F-actin undergoes rapid and reversible redistribution and intercellular gap formation for both cases.

For the static case where the cells were cultured on cover slips, detailed orientation of F-actin fibers and cell-cell gap formation were visible (Figure 5). After 20 min of thrombin treatment, the actin had reorganized into prominent stress fibers aligned parallel to each other and to the long axis of the cell. Compared to the control case, the cells had retracted from one another and exhibited small gaps between adjacent cells while retaining their polygonal

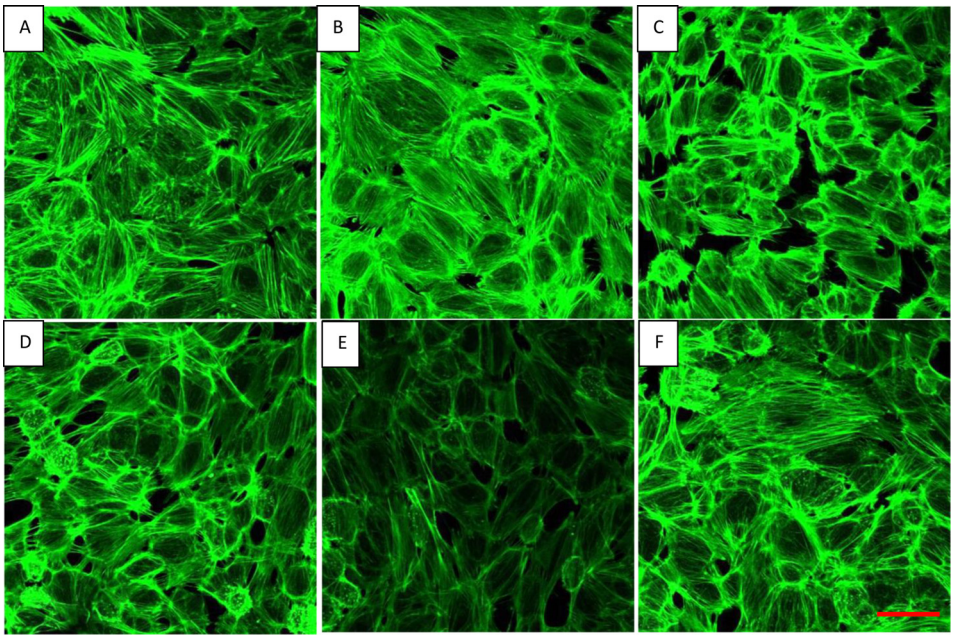

FIG. 6. Confocal Z-projections of thrombin induced F-actin remodeling on BAOECs cultured under static conditions on a cover slip. (a) Control case not subjected to thrombin treatment. Note the tight intercellular contact and predominantly peripheral cortical actin staining. (b) 20 min of thrombin treatment at 1 U/ml appear to induce intercellular gap formation and marked increase in actin stress fiber formation. (c) 40 min of thrombin treatment at 1 U/ml increases intercellular gap formation and produces notable decrease in cell size possibly due to acto-myosin based cell contraction. (d) 60 min of thrombin treatment at 1 U/ml seems to reduce intercellular gaps. (e) 80 min of thrombin treatment at 1 U/ml have significantly reduced intercellular gaps and there is significant decrease in F-actin stress fiber presence. (f) 100 min of thrombin treatment at 1 U/ml produce cell characteristics comparable to control case (Scale bar: 25 μm).

morphology. The ECs still remained attached to one another and, in many areas, the stress fibers appeared to be contiguous between adjacent cells. 40 min of thrombin treatment increased intercellular gaps and produced a notable decrease in cell size, possibly due to acto-myosin based cell contraction. There was a reduction in intercellular gaps and a recovery in thrombin based inflammatory response by 60 min of treatment. 80 min of thrombin treatment produced cell monolayers with significantly reduced intercellular gaps coupled with a significant decrease in the presence of F-actin stress fibers within the cell's cytoplasm. The 100 min case had cell characteristics comparable to that of the control (no thrombin treatment) case.

The BBV platform is thin enough to allow imaging of the ECs at 60× magnification using an oil immersion objective. However, the presence of multiple layers (glass, PDMS, membrane) of different refractive indices between the cell and the objective resulted in images that were compromised on details. Stress fiber presence and orientation were not well described in these images, but details on cell-cell gap formation were available (Figure 6). 20 min of thrombin treatment on ECs under flow resulted in intercellular regions lacking F-actin stress fibers, which signify intercellular gap formation. After 40 min, these gaps decreased in size and frequency of appearance. The gaps might be reduced by increased cortical actin presence towards cell peripheries. Further thrombin treatment (60 min) led to a uniform F-actin presence throughout the cell monolayer with reduced intercellular gaps, which was comparable to the control case.

Our results on static cover slip studies are comparable to the established literature. Thrombin stimulation initially causes polymerization of actin fibers in ECs that organize into thick stress fibers and are arranged parallel to each other, leading to intercellular gap formation.[51] Further treatment is known to decrease the F-actin quantity and return to the control case (no thrombin) level.[54] Quantifying F-actin content in thrombin activated ECs has shown an increase in actin polymerization during the initial 30 min of thrombin treatment followed by a reduction in total F-actin content by 60 min.[51]

Analysis of Figures 5 and 6 provided a quantitative understanding of the relative increase in intercellular gap area for BBV and static transwell cases. The max increase in intercellular gap area for the BBV model and transwell insert model was 11.1% (from 20 min image scan) and 14.8% (from 40 min image scan), respectively (Figure 7). We found the calculated values from image analysis to fall close to the predicted range from our permeability model (12%–15%). We do understand that these are only F-actin stained images and not images of any intercellular junction protein like VE-Cadherin, and still it does provide a quantitative factor to the qualitative characterization of the images.

Comparison to computational model

To better understand the molecular diffusion from a theoretical perspective, a computational model of the molecular transport in the microfluidic BBV model was built, as illustrated in Figure S1, supplementary material. The tracer molecule concentration in the bi-layer device and its transport mechanism can be simulated and well predicted using this computational model. In Figure S2, supplementary material, the distribution of molecule mimicking particles provides a better understanding of the molecule transport dynamics. Specifically, molecules in the apical channel mainly follow a parabolic flow pattern with a slight disturbance induced by Brownian Motion, while molecules in the basal channel are predominantly the ones that have diffused through the porous membrane. The time history of the average molecular concentration in the bottom channel for membranes with equivalent pore diameters of 200 nm, 400 nm, 800 nm, and 1 μm is also shown in Figure S3, supplementary material. Here, the equivalent pore diameter takes into account the effect of both membrane pores and intercellular gaps. It is observed that it takes a longer time for larger molecules to transport across the membrane with smaller equivalent pore diameters. The smaller diffusion coefficient of larger molecules combined with higher flow resistance from small pores significantly reduces the dye transport rate across the membrane. It is shown in Fig. S3, supplementary material, that for cases with 800 nm and 1 μm equivalent diameter pores, the concentration trends of these three molecules are almost identical, which indicates that the transport rate is nearly independent of diffusion coefficient. Thus, it can be concluded that molecule transport across the membrane with large pore sizes is convection dominant. As the equivalent pore diameter decreases to 400 nm or 200 nm, the difference between their concentrations trends becomes more significant. This indicates that diffusion and convection are both influential in dye transport across the membrane. The experimental results in Figure 2(d) demonstrate up to a 2–6 fold difference for these three molecules, which suggests that the diffusion induced transport contributes significantly to the abluminal concentration. In other words, the actual intercellular gap size in the cell layer should be smaller than 400 nm, which is much smaller than the 1 μm pores on the membrane.

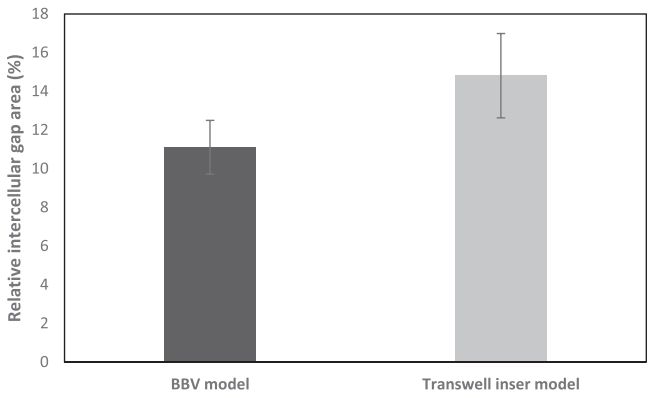

FIG. 7. Relative increase in intercellular gap area for BBV and static transwell case calculated from confocal images in Figures 5 and 6. The max increase in intercellular gap area for BBV model and transwell insert model was 11.1% (from 20 min image scan) and 14.8% (from 40 min image scan). Sample size n = 10 images for each case.

Our simulation results can also provide guidance on estimation of average pore size during thrombin treatment. In the time scale of the experimental tests, the abluminal concentration increases approximately linearly, provided the pore size was constant which is indicated from the zoomed-in image of Fig. S3, supplementary material. Specifically, taking our experimental results as an example: in 20 min FITC dye and FITC Dextran 4k Da increase ∼4.0 and ∼5.2 times faster than FITC Dextran 70k Da, respectively. Although cells experience a dynamic process under thrombin treatment and gap sizes constantly change over time, the equivalent pore size at the 20-min time point can be roughly estimated between 200 nm and 400 nm by referring to the linear correlation. Future live observations of intercellular gap size change will be performed using fluorescent scans and AFM measurements to validate this hypothesis.

CONCLUSION

Traditional *in vitro* studies can provide a biological approximation of vascular permeability but cannot account for the true nature due to the lack of a holistic system.[55,56] An *in vivo* intact endothelium is exposed to multiple factors and is differentially regulated in space and time.[55,57] Current *in vitro* platforms for studying EC biology and permeability have limitations in incorporating these numerous and dynamic factors. Our BBV model cultures ECs under biomimetic flow conditions and we can expose cells to multiple external cues in a spatially and temporally controlled manner from the basal and/or apical side to understand their responses towards a heterogeneous environment. In this work, we examined the permeability of ECs when treated with thrombin in BBV and traditional transwell insert models. Real time data collection and analytical permeability models allowed us to compare the dynamics of thrombin induced EC layer permeability for different tracer molecules and their permeability characteristics between the two platforms.

From the permeability data of the three tracer molecules, it can be concluded that the amount of tracer molecule transported through the cells and membrane layer is inversely proportional to the tracer molecule size. FITC sodium salt (376 Da) had the highest permeability followed by FITC-Dextran 4k Da and FITC-Dextran 70k Da, respectively (Figures 2(d) and 3(a)). By analyzing the permeability data, we concluded that the dynamics and extent of endothelial layer permeability is similar when cultured under flow and static conditions. FITC-Dextran 4k Da with diffusion dominated transport characteristics (Peclet number <1) has similar quantity of tracer molecules diffusing to the lower channel in both platforms as the small sized tracer molecule is not influenced by the convective flow. Conversely, the bigger FITC-Dextran 70k Da (Peclet number ~1) tracer molecule has about 2 times more tracer molecule transported to the lower channel in the BBV model compared to the transwell case (Figure 4(a)). This is not because of an excess increase in intercellular gap area in the BBV model compared to transwell static case, as we had confirmed the relative intercellular gap area to be similar between the two platforms using our analytical model (Figure 4(b)) alongside F-actin stained immunofluorescence image analysis (Figure 7). From the permeability data, a relative intercellular area increase of ∼12%–15% for both the diffusion dominated FITC and FITC-Dextran 4k Da tracer molecules is predicted and this value is closely matched from the fluorescence image data, which finds the max increase in intercellular gap area for BBV model and transwell insert models to be 11.1% and 14.8%, respectively. By using a computational model of the BBV model, we also predict a possible dimension range for the intercellular gap formed on the EC layer. From the simulation results, the average intercellular gap size should be smaller than 400 nm.

Our current work suggests that for studies involving relatively larger molecules/elements (like proteins, antibodies, particles etc.) *in vitro* blood vessel models where ECs are cultured/tested under *in vivo* levels of flow are more appropriate. The transport, binding, appearance, arrangement, release, and clearance characteristics of these molecules/elements will be influenced by the effect of fluid flow shear on them. Thus, the data generated using these more biomimetic *in vitro* testing platforms, like our BBV system, would be more credible and will carry more value. Also, the phenotype and function of ECs *in vivo* are influenced by complex

mechanical signals generated by the FSS they are exposed to. This makes our BBV system a more physiologically relevant *in vitro* model compared to traditional transwell inserts despite only being comprised of a monolayer of ECs. Also, a microfluidics based platform is easy to fabricate, cost-effective, needs minimum reagent volumes, and allows for real time imaging. Our future *in vitro* blood vessel models will have the relevant support cell systems (smooth muscle cells/pericyte) and an extracellular matrix scaffold to answer related questions in vascular biology. These additions will take the model a step closer towards modeling *in vivo* systems while helping to bridge the gap between *in vitro* and *in vivo* studies.

SUPPLEMENTARY MATERIAL

See supplementary material for more details on computational model based analysis of tracer molecule transport and technique used for collecting tracer molecule in the bi-layer device

ACKNOWLEDGMENTS

This work was supported by National Science Foundation (NSF) CAREER Grant Nos. CBET-1113040, NSF DMS-1516236, NSF CBET-1067502, NSF CBET 1264808, and National Institutes of Health (NIH) Grant Nos. R01HL131750, EB015105, The Pennsylvania Infrastructure Technology Alliance (PITA) program and Alternatives Research & Development Foundation.

The authors would like to thank Christopher Uhl for research assistance and for critical manuscript review. Research from the Liu laboratory present herein was initiated with support from the Biosystems Dynamics Summer Institute, funded through an HHMI undergraduate education grant to Lehigh University.

[1]H. F. Dvorak *et al.*, "Vascular permeability factor/vascular endothelial growth factor, microvascular hyperpermeability, and angiogenesis," Am. J. Pathol. **146**(5), 1029–1039 (1995).
[2]A. A. Miles and E. M. Miles, "Vascular reactions to histamine, histamine-liberator and leutaxine in the skin of guinea pigs," J. Physiol. **118**(2), 228–257 (1952).
[3]S. M. Weis, "Vascular permeability in cardiovascular disease and cancer," Curr. Opin. Hematol. **15**(3), 243–249 (2008).
[4]P. Kumar *et al.*, "Molecular mechanisms of endothelial hyperpermeability: Implications in inflammation," Expert Rev. Mol. Med. **11**, e19 (2009).
[5]G. P. van Nieuw Amerongen *et al.*, "Transient and prolonged increase in endothelial permeability induced by histamine and thrombin: Role of protein kinases, calcium, and RhoA," Circ. Res. **83**(11), 1115–1123 (1998).
[6]R. S. Cotran and G. Majno, "The delayed and prolonged vascular leakage in inflammation. I. Topography of the leaking vessels after thermal injury," Am. J. Pathol. **45**, 261–281 (1964).
[7]R. S. Cotran, "The delayed and prolonged vascular leakage in inflammation. II. An electron microscopic study of the vascular response after thermal injury," Am. J. Pathol. **46**, 589–620 (1965).
[8]J. Nagy *et al.*, "Vascular permeability, vascular hyperpermeability and angiogenesis," Angiogenesis **11**(2), 109–119 (2008).
[9]M.-J. Rabiet *et al.*, "Thrombin-induced increase in endothelial permeability is associated with changes in cell-to-cell junction organization," Arterioscler., Thromb., Vasc. Biol. **16**(3), 488–496 (1996).
[10]N. Shanks, R. Greek, and J. Greek, "Are animal models predictive for humans?," Philos., Ethics, Humanit. Med. **4**(1), 2 (2009).
[11]C. A. Staton *et al.*, "Current methods for assaying angiogenesis *in vitro* and *in vivo*," Int. J. Exp. Pathol. **85**(5), 233–248 (2004).
[12]J. A. Cooper *et al.*, "Measurement of albumin permeability across endothelial monolayers *in vitro*," J. Appl. Physiol. **62**, 1076–1083 (1987).
[13]S. Kerkar *et al.*, "TNF-α and IL-1β increase pericyte/endothelial cell co-culture permeability," J. Surg. Res. **132**(1), 40–45 (2006).
[14]K. S. Mark and D. W. Miller, "Increased permeability of primary cultured brain microvessel endothelial cell monolayers following TNF-α exposure," Life Sci. **64**(21), 1941–1953 (1999).
[15]S. M. Albelda *et al.*, "Permeability characteristics of cultured endothelial cell monolayers," J. Appl. Physiol. **64**, 308–322 (1988).
[16]P. J. Del Vecchio, A. Siflinger-Birnboim, J. M. Shepard, R. Bizios, J. A. Cooper, and A. B. Malik, "Endothelial monolayer permeability to macromolecules," Fed. Proc. **46**(8), 2511–2515 (1987).
[17]E. W. Young *et al.*, "Technique for real-time measurements of endothelial permeability in a microfluidic membrane chip using laser-induced fluorescence detection," Anal. Chem. **82**(3), 808–816 (2010).
[18]Y. Kim *et al.*, "Probing nanoparticle translocation across the permeable endothelium in experimental atherosclerosis," Proc. Natl. Acad. Sci. U.S.A. **111**(3), 1078–1083 (2014).
[19]S. Srigunapalan *et al.*, "A microfluidic membrane device to mimic critical components of the vascular microenvironment," Biomicrofluidics **5**(1), 013409 (2011).
[20]P. F. Davies, T. Mundel, and K. A. Barbee, "A mechanism for heterogeneous endothelial responses to flow *in vivo* and *in vitro*," J. Biomech. **28**(12), 1553–1560 (1995).
[21]D. E. Ingber, "Mechanical signaling and the cellular response to extracellular matrix in angiogenesis and cardiovascular physiology," Circ. Res. **91**(10), 877–887 (2002).

[22]J. Y.-J. Shyy and S. Chien, "Role of integrins in endothelial mechanosensing of shear stress," Circ. Res. **91**(9), 769–775 (2002).
[23]D. Mehta and A. B. Malik, "Signaling mechanisms regulating endothelial permeability," Physiol. Rev. **86**(1), 279–367 (2006).
[24]W. M. Kuebler, X. Ying, and J. Bhattacharya, "Pressure-induced endothelial Ca^{2+} oscillations in lung capillaries," Am. J. Physiol. **282**(5), L917–L923 (2002).
[25]M. U. Nollert, S. G. Eskin, and L. V. McIntire, "Shear stress increases inositol trisphosphate levels in human endothelial cells," Biochem. Biophys. Res. Commun. **170**(1), 281–287 (1990).
[26]G. Schwarz *et al.*, "Shear stress-induced calcium transients in endothelial cells from human umbilical cord veins," J. Physiol. **458**, 527–538 (1992).
[27]Y. L. Hu *et al.*, "Roles of microtubule dynamics and small GTPase Rac in endothelial cell migration and lamellipodium formation under flow," J. Vasc. Res. **39**(6), 465–476 (2002).
[28]E. Tzima *et al.*, "Activation of Rac1 by shear stress in endothelial cells mediates both cytoskeletal reorganization and effects on gene expression," EMBO J. **21**, 6791–6800 (2002).
[29]K. G. Birukov *et al.*, "Magnitude-dependent regulation of pulmonary endothelial cell barrier function by cyclic stretch," Am. J. Physiol. **285**(4), L785–L797 (2003).
[30]A. Thomas *et al.*, "Biomimetic channel modeling local vascular dynamics of pro-inflammatory endothelial changes," Biomicrofluidics **10**(1), 014101 (2016).
[31]E. Tzima *et al.*, "Activation of integrins in endothelial cells by fluid shear stress mediates Rho-dependent cytoskeletal alignment," EMBO J. **20**(17), 4639–4647 (2001).
[32]T. G. Papaioannou and C. Stefanadis, "Vascular wall shear stress, basic principles and methods," Hellenic J. Cardiol. **46**(1), 9–15 (2005).
[33]Y. Son, "Determination of shear viscosity and shear rate from pressure drop and flow rate relationship in a rectangular channel," Polymer **48**(2), 632–637 (2007).
[34]D. A. Baron *et al.*, "Atriopeptin inhibition of thrombin-mediated changes in the morphology and permeability of endothelial monolayers," Proc. Natl. Acad. Sci. U.S.A. **86**(9), 3394–3398 (1989).
[35]R. A. Stockton, E. Schaefer, and M. A. Schwartz, "p21-activated kinase regulates endothelial permeability through modulation of contractility," J. Biol. Chem. **279**(45), 46621–46630 (2004).
[36]K. W. Buchan and W. Martin, "Modulation of barrier function of bovine aortic and pulmonary artery endothelial cells, dissociation from cytosolic calcium content," Br. J. Pharmacol. **107**(4), 932–938 (1992).
[37]G. P. van Nieuw Amerongen *et al.*, "GIT1 mediates thrombin signaling in endothelial cells: Role in turnover of RhoA-type focal adhesions," Circ. Res. **94**(8), 1041–1049 (2004).
[38]O. Kedem and A. Katchalsky, "Permeability of composite membranes. Part 1.—Electric current, volume flow and flow of solute through membranes," Trans. Faraday Soc. **59**, 1918–1930 (1963).
[39]S. Q. Wang *et al.*, "Computational modeling of magnetic nanoparticle targeting to stent surface under high gradient field," Comput. Mech. **53**(3), 403–412 (2014).
[40]N. Periasamy and A. S. Verkman, "Analysis of fluorophore diffusion by continuous distributions of diffusion coefficients: Application to photobleaching measurements of multicomponent and anomalous diffusion," Biophys. J. **75**(1), 557–567 (1998).
[41]T. Kihara, J. Ito, and J. Miyake, "Measurement of biomolecular diffusion in extracellular matrix condensed by fibroblasts using fluorescence correlation spectroscopy," PLoS One **8**(11), e82382 (2013).
[42]J. Seebach *et al.*, "Endothelial barrier function under laminar fluid shear stress," Lab. Invest. **80**(12), 1819–1831 (2000).
[43]J. Seebach *et al.*, "Regulation of endothelial barrier function during flow-induced conversion to an arterial phenotype," Cardiovasc. Res. **75**(3), 598–607 (2007).
[44]R. Stockton *et al.*, "Induction of vascular permeability: βPIX and GIT1 scaffold the activation of extracellular signal-regulated kinase by PAK," Mol. Biol. Cell **18**(6), 2346–2355 (2007).
[45]Y. S. Chang *et al.*, "Effect of vascular endothelial growth factor on cultured endothelial cell monolayer transport properties," Microvasc. Res. **59**(2), 265–277 (2000).
[46]A. Hoffmann *et al.*, "High and Low Molecular Weight Fluorescein Isothiocyanate (FITC)–dextrans to assess blood-brain barrier disruption: Technical considerations," Transl. Stroke Res. **2**(1), 106–111 (2011).
[47]G. Sahagun, S. A. Moore, and M. N. Hart, "Permeability of neutral vs. anionic dextrans in cultured brain microvascular endothelium," Am. J. Physiol. **259**, H162–H166 (1990).
[48]P. Gribbon and T. E. Hardingham, "Macromolecular diffusion of biological polymers measured by confocal fluorescence recovery after photobleaching," Biophys. J. **75**(2), 1032–1039 (1998).
[49]J. D. Bryers and F. Drummond, "Local macromolecule diffusion coefficients in structurally non-uniform bacterial biofilms using fluorescence recovery after photobleaching (FRAP)," Biotechnol. Bioeng. **60**(4), 462–473 (1998).
[50]C. Tiruppathi *et al.*, "Synergistic effects of tumor necrosis factor-α and thrombin in increasing endothelial permeability," Am. J. Physiol. **281**, L958–L968 (2001).
[51]Z. M. Goeckeler and R. B. Wysolmerski, "Myosin light chain kinase-regulated endothelial cell contraction: The relationship between isometric tension, actin polymerization, and myosin phosphorylation," J. Cell Biol. **130**(3), 613–627 (1995).
[52]R. Sandoval *et al.*, "Requirement for Ca^{2+} signaling in the mechanism of thrombin-induced increase in endothelial permeability," Amer. J. Physiol. - Lung Cellular Mol. Physiol. **280**, L239–L247 (2001).
[53]R. B. Wysolmerski and D. Lagunoff, "Involvement of myosin light-chain kinase in endothelial cell retraction," Proc. Natl. Acad. Sci. U.S.A. **87**(1), 16–20 (1990).
[54]I. B. Alieva *et al.*, "The leading role of microtubules in endothelial barrier dysfunction: Disassembly of peripheral microtubules leaves behind the cytoskeletal reorganization," J. Cell. Biochem. **114**(10), 2258–2272 (2013).
[55]W. C. Aird, "Endothelial cell dynamics and complexity theory," Crit. Care Med. **30**(5), S180–S185 (2002).
[56]T. Minami *et al.*, "Thrombin and phenotypic modulation of the endothelium," Arterioscler., Thromb., Vasc. Biol. **24**(1), 41–53 (2004).
[57]W. C. Aird, "Endothelial cell heterogeneity," Crit. Care Med. **31**(4), S221–S230 (2003).